Treatment of competition between complete fusion and quasifission in collisions of heavy nuclei

G.G.Adamian[1,2], N.V.Antonenko[1,2], W.Scheid[1] and V.V.Volkov[2]

[1] *Institut für Theoretische Physik der Justus–Liebig–Universität, D–35392 Giessen, Germany*

[2] *Joint Institute for Nuclear Research, 141980 Dubna, Russia*

(February 9, 2008)

Abstract

A model of competition between complete fusion and quasifission channels in fusion of two massive nuclei is extended to include the influence of dissipative effects on the dynamics of nuclear fusion. By using the multidimensional Kramers-type stationary solution of the Fokker–Planck equation, the fusion rate through the inner fusion barrier in mass asymmetry is studied. Fusion probabilities in symmetric ^{90}Zr+^{90}Zr, ^{100}Mo+^{100}Mo, ^{110}Pd+^{110}Pd, ^{136}Xe+^{136}Xe, almost symmetric ^{86}Kr+^{136}Xe and ^{110}Pd+^{136}Xe reactions are calculated. An estimation of the fusion probabilities is given for asymmetrical ^{62}Ni+^{208}Pb, ^{70}Zn+^{208}Pb, ^{82}Se+^{208}Pb, and ^{48}Ca+^{244}Pu reactions used for the synthesis of new superheavy elements.

PACS:25.70.Jj, 24.10.-i, 24.60.-k

Key words: Complete fusion; Quasifission; Compound nucleus; Superheavy nuclei

I. INTRODUCTION

The competition between the complete fusion and quasifission processes occurs in the reactions with massive nuclei at bombarding energies smaller than 15 MeV/nucleon. In these reactions the quasifission channel dominates and leads to a strong reduction of few orders of magnitude of the fusion cross section σ_{CN} [1]. The competition between the complete fusion and quasifission processes was not considered in the calculations with various models, namely with the macroscopic dynamical [2], optical [3] and surface friction [4] models. It was shown in [1] that these models do not lead to correct fusion cross sections for reactions with heavy nuclei [5–7]. The new model suggested in [1] yields a good agreement between the theoretical predictions and experimental data on the fusion of heavy nuclei. Within this model the fusion cross section σ_{CN} is defined as

$$\sigma_{CN}(E_{\rm c.m.}) = \sum_{J=0}^{J_{max}} \sigma_c(E_{\rm c.m.}, J) P_{CN}(E_{\rm c.m.}, J). \quad (1)$$

Here, σ_c is the capture cross section at the bombarding energy $E_{\rm c.m.}$ and angular quantum number J and P_{CN} the fusion probability after the capture stage of collision, which takes the competition between the fusion and quasifission processes into account. The value of J_{max} depends on $E_{\rm c.m.}$ and is smaller than $J_{B_f=0}$ at which the fission barrier in the compound nucleus vanishes [8]. In order to calculate σ_c, either optical [3] or surface friction [4] models can be used [1]. $P_{CN} = 1$ is supposed in the models of Refs. [3,4]. In the macroscopic dynamical model [2] $P_{CN} = 1$ for $E_{\rm c.m.} > B_C + E_{\rm xx}$ and $P_{CN} = 0$ for $E_{\rm c.m.} < B_C + E_{\rm xx}$ where B_C and $E_{\rm xx}$ are the Coulomb barrier and the extra–extra push energy, respectively. The main advantage of the model [1] in contrast to the models [2–4] is the treatment of the competition between the complete fusion and quasifission in the calculation of P_{CN}. In the present paper the model [1] is extended by including dissipative effects on the fusion dynamics.

The fusion process is considered in [1] as the evolution of the dinuclear system (DNS) in which nucleons are transfered from the light nucleus to the heavy one [9]. The DNS-concept

is based on the information obtained from the investigation of deep inelastic collisions of heavy ions [10]. The DNS is formed at the initial stage of the reaction when the kinetic energy is transformed into the excitation energy of the nuclei. The initial DNS is localized in the minimum of the pocket of the nucleus-nucleus potential $V(R)$ (Fig. 1) at $R = R_m$ where R is the relative distance between the interacting nuclei. In our approach we have $R_m \approx R_1+R_2+0.5$ fm where R_1 and R_2 are the radii of the nuclei in the DNS. Then the DNS evolves by a diffusion process in the mass asymmetry degree of freedom $\eta = (A_1 - A_2)/A$ to the compound nucleus and fuses (Fig. 1). A_1 and A_2 are the mass numbers of the nuclei and $A = A_1 + A_2$. Besides the motion in η a diffusion process in the relative distance occurs. This process leads to the decay of the DNS which we denote as quasifission. For quasifission the DNS should overcome the potential barrier (B_{qf}) which coincides with the depth of the pocket in the potential $V(R)$ (Fig. 1). The important peculiarity of the DNS evolution to the compound nucleus is the appearance of an inner fusion barrier B^*_{fus} in the mass asymmetry degree of freedom with its top (the Businaro-Gallone point) at $\eta = \eta_{BG}$ which coincides with the maximum of the DNS potential energy as a function of η (Fig. 1). The value of B^*_{fus} supplies the hindrance for the complete fusion in the DNS-concept. The energy required to overcome the fusion barrier B^*_{fus} is contained in the DNS excitation energy. As was found in [1,11,12], the value of B^*_{fus} can be much smaller than the extra-extra push energy predicted in [2].

The dissipative large-amplitude collective nuclear motions, which occur in fission, quasifission, fusion and heavy-ion reactions, can be analyzed within the transport theory. It is known that the Kramers expression [14] yields an excellent approximation to the fission rate in comparison to the solution of the Fokker-Planck and Langevin equations [15,20,16]. The fusion probability P_{CN} (1) can be obtained with the Kramers-type expression for the rate of fusion through the inner fusion barrier. The main advantage of the Kramers-type expression for the fusion rate in contrast to the statistical method [1] is the possibility to include nuclear viscosity in fusion process. In this paper, the two-dimensional (R and η) Kramers-type expression is applied to the calculation of P_{CN}. In the following we analyt-

ically demonstrate the dependence of the fusion probability on the values of the friction coefficients, the temperature T of the DNS, and the values of B^*_{fus} and B_{qf}. As examples, the symmetrical, almost symmetrical, and asymmetrical reactions will be considered.

II. MODEL

A. Fusion probability

The variables R and η are the relevant collective variables used in [1,17] to describe the DNS evolution. The neck degree of freedom [2,18,19] which is important in macroscopic dynamical models is not considered in this paper. As follows from our analysis [19], the neck is not a relevant collective variable for values of $R > R_1 + R_2$ which are important in the DNS. The size of the neck in the liquid drop model and the overlap region in the frozen density approximation are close to each other for $R_1 + R_2 \leq R \leq R_1 + R_2 + 1\,\mathrm{fm}$ [19]. Based on this fact and the time scale, which is of interest, we assume that the individuality of the DNS nuclei in the fusion process is retained, and follow the approach suggested in [1,12].

Since the fusion probability increases with the mass asymmetry, the DNS with larger mass asymmetry supplies favorable conditions for complete fusion. We assume that the fusion occurs inevitably for $\eta > \eta_{BG}$. The diffusion in η is important in our consideration of the fusion process. The simultaneous investigation of the transport processes in η and R variables allows us to calculate the fusion and quasifission probabilities [12]. In our opinion, the fusion probability is small in many reactions with heavy nuclei because the initial mass asymmetry η_i is smaller than η_{BG} and the diffusion in η is much smaller than the diffusion in R.

The leakage of probability through the fusion barrier in η is defined by the rate $\lambda_\eta(t)$ at $\eta = \eta_{BG}$ (Fig. 1). Then we obtain

$$P_{CN} = \int_0^{t_0} \lambda_\eta(t) dt \tag{2}$$

Here, t_0 is the life-time of the DNS with

$$\int_0^{t_0}[\lambda_R(t)+\lambda_\eta(t)]dt = 1. \tag{3}$$

For symmetrical and almost symmetrical systems, the symmetry of the fusion process with respect to $\eta = 0$ should be taken into account. Then the initial DNS is near the minimum of the potential energy $U(\eta)$ which is a symmetric function with respect to $\eta = 0$ (Fig. 1). Fusion occurs when DNS reaches the barriers at either $\eta = \eta_{BG}$ or $\eta = -\eta_{BG}$. The time dependence of the rates $\lambda_i(t)$ $(i = R, \eta)$ can be taken in the following way

$$\lambda_i(t) = \lambda_i^{Kr}\left(\frac{e^{t/\tau_i}-1}{e-1}\theta(\tau_i - t) + \theta(t-\tau_i)\right), \tag{4}$$

where λ_i^{Kr} are asymptotic values of the fusion or quasifission rate $\lambda_i(t)$ at the corresponding barriers (Fig. 1) and $\theta(t)$ is a step function. Here, we assume that after the exponential growth during the transient time τ_i the rate $\lambda_i(t)$ reaches the asymptotic value.

Using (4) we obtain from Eqs. (2) and (3)

$$P_{CN} = P_{CN}^0 - \Delta P_{CN} = \frac{\lambda_\eta^{Kr}}{\lambda_R^{Kr}+\lambda_\eta^{Kr}} - \frac{\lambda_\eta^{Kr}\lambda_R^{Kr}}{\lambda_R^{Kr}+\lambda_\eta^{Kr}}\frac{\tau_\eta - \tau_R}{\beta}, \tag{5}$$

$$t_0 = t_{00} + \Delta t = \frac{1}{\lambda_R^{Kr}+\lambda_\eta^{Kr}} + \frac{\lambda_R^{Kr}\tau_R + \lambda_\eta^{Kr}\tau_\eta}{(\lambda_R^{Kr}+\lambda_\eta^{Kr})\beta}, \tag{6}$$

where $\beta = e - 1 \approx 1.72$. Assuming instead of (4) the linear grows of $\lambda_i(t)$ [13]

$$\lambda_i(t) = \lambda_i^{Kr}\left(\frac{t}{\tau_i}\theta(\tau_i - t) + \theta(t-\tau_i)\right) \tag{7}$$

we obtain the Eqs. (5) and (6) but with $\beta = 2$. The first terms in (5) and (6) are the contributions from the quasistationary rates. The second terms are related to the transient time. One can see from (5) that we can neglect the transient time for $\tau_i \ll 1/\lambda_i^{Kr}$ $(i = R, \eta)$ or $\tau_R \approx \tau_\eta$. This is true for all reactions under consideration excepting the ^{136}Xe+^{136}Xe and ^{110}Pd+^{136}Xe reactions where the differences between B_{fus}^* and B_{qf} are very large. Note that the role of the transient stage decreases with decreasing excitation energy of the DNS because the exponential increase of $1/\lambda_R^{Kr}$ is larger than the logarithmic increase of the transient times (see equations below).

To obtain the asymptotic fusion and quasifission rates λ_i^{Kr} $(i = R, \eta)$, we use the formalism elaborated in Refs. [15,16]. We approximate the expression for the quasistationary rate λ_i^{Kr} over a multidimensional potential barrier [16] with a Kramers-type formula

$$\lambda_i^{Kr} = \frac{1}{2\pi}\frac{\omega_i^2}{\sqrt{\omega_i^{B_R}\omega_i^{B_\eta}}}\left(\sqrt{\left[\frac{(\Gamma/\hbar)^2}{\omega_i^{B_R}\omega_i^{B_\eta}}\right]^2+4}-\frac{(\Gamma/\hbar)^2}{\omega_i^{B_R}\omega_i^{B_\eta}}\right)^{1/2}\exp\left[-\frac{B_i}{T}\right]. \quad (8)$$

Here, B_i $(i = R, \eta)$ defines the height of the fusion $(B_\eta = B^*_{fus})$ or quasifission $(B_R = B_{qf})$ barriers. The possibility to apply the Kramers-type expression to relatively small barriers $(B_i/T > 0.5)$ was demonstrated in [20]. The local thermodynamic temperature T is calculated with the expression $T = \sqrt{E^*/a}$, where $a = A/12$ MeV^{-1} and E^* is the DNS excitation energy. In Eq. (8), the frequencies $\omega_i^{B_j}$ $(j = R, \eta)$ of the inverted harmonic oscillators approximate the potential in the variables $i = R, \eta$ on the tops of the barriers B_j, and ω_i are the frequencies of the harmonic oscillators approximating the potential in the same variables for the initial DNS. Since the local oscillator approximation of the potential energy surface is good for the reaction considered, we neglected the nondiagonal components of the curvature tensors in (8). In our calculations, we use the simple approximate expressions for the friction coefficients

$$\gamma_{ii'} = \Gamma\mu_{ii'}/\hbar, \quad (i, i' = R, \eta),$$

which were obtained by the linear response theory [21]. The quantity Γ denotes an average double width of the single-particle states. The calculation of the mass parameters μ_{RR} and $\mu_{\eta\eta}$ is given in [12,22]. The role of the nondiagonal components of the tensors of inertia and friction depends very much on the choice of the collective variables [21,22]. By using the collective variables R and η for describing the evolution of the DNS we neglect the nondiagonal component of the tensor of inertia because $\mu_{R\eta} \ll \sqrt{\mu_{RR}\mu_{\eta\eta}}$ for $|\eta| < |\eta_{BG}|$ [22]. The nondiagonal mass coefficient $\mu_{R\eta} = 0$ in the DNS takes an essential role only for $|\eta| > |\eta_{BG}|$. As was shown in [12,19], the friction coefficients γ_{RR} and $\gamma_{\eta\eta}$ obtained with $\Gamma = 2$ MeV have the same order of magnitude as the ones calculated within the other approaches.

B. Potential energy of the DNS

The value of

$$\omega_i^{B_j} = \sqrt{\left|\frac{\partial^2 U(R,\eta,J)}{\partial i^2}\right|_{B_j}/\mu_{ii}}$$

is easily calculated with the potential energy of the DNS

$$U(R,\eta,J) = B_1 + B_2 + V(R,J) - [B_{12} + V_{rot}^{'}(J)]. \quad (9)$$

Here, B_1, B_2, and B_{12} are the binding energies of the fragments and the compound nucleus and are calculated with liquid-drop masses for large excitation energies and with realistic masses [23] for small excitation energies. The isotopic composition of the nuclei forming the DNS is chosen with the condition of a N/Z-equilibrium in the system. The value of $U(R,\eta,J)$ is normalized to the energy of the rotating compound nucleus by $B_{12}+V_{rot}^{'}$. The nucleus-nucleus potential $V(R,J)$ in (9) is calculated as described in [24]. The retaining individuality of the DNS nuclei during the time which is of interest allows us to calculate the DNS potential energy by the method presented in [24]. The calculated driving potential $U(R_m,\eta,J=0) = U(\eta)$ as a function of η and the nucleus–nucleus potential $V(R,J=0)$ as a function of R in the reaction ^{90}Zr + ^{90}Zr is presented in Fig. 1.

The potential energy of the DNS as a function of η and R depends on the temperature, shell effects and angular momentum. In the present paper we do not analyse in details the dependence of the potential energy surface on temperature because this demands the introduction of an additional parameter. We distinguish two cases: The first case corresponds to large excitation energies of the initial DNS when the liquid drop binding energies and spherical shapes of the nuclei in the DNS can be used in the calculations. The second case corresponds to the cold fusion with small E^* when the realistic binding energies are taken in (9). For small values of E^*, the deformation of the nuclei in their ground states [25] is taken in the DNS into account when the barrier heights are calculated. In order to demonstrate the influence of the shell and deformation effects at small E^*, the calculation of $U(R_m,\eta,J=0)$ is presented in Fig. 2 for the ^{86}Kr+^{136}Xe reaction. In this reaction the

deformation of the nuclei in the DNS leads to a decrease of B^*_{fus}. After the smoothing over small oscillations caused by even-odd effects we can use the expression (8) for λ_i^{Kr} in first approximation. The calculated driving potentials for the reactions leading to superheavy nuclei are presented in [26]. Below we discuss the case of the ^{86}Kr+^{136}Xe reaction where the fusion probability is calculated with driving potentials based on spherical and deformed shapes of the nuclei. The calculations of complete fusion probabilities with spherical (the liquid drop binding energies) and deformed (the realistic binding energies) nuclei give us the interval where realistic values of P_{CN} are situated. As noted in Ref. [12], the values of P_{CN} for small E^* can be smaller or larger than the ones for large E^*. In our calculations of the fusion probability, the following values $\hbar\omega_R^{B_R} \approx 0.8 - 1$ MeV, $\hbar\omega_R^{B_\eta} \approx 3 - 3.5$ MeV, $\hbar\omega_\eta^{B_R} \approx 1 - 1.5$ MeV, $\hbar\omega_\eta^{B_\eta} \approx 1.5 - 2$ MeV, $\hbar\omega_R \approx 1.5 - 2$ MeV, and $\hbar\omega_\eta \approx 0.8 - 1$ MeV are used for the reactions considered.

The dependences of the barrier heights on J for the reactions ^{90}Zr+^{90}Zr and ^{110}Pd+^{110}Pd are presented in Fig. 3. The values of B^*_{fus} and B_{qf} are slightly changed when J increases from 0 to 25$\hbar$. For heavier systems, this changes are certainly smaller because of the larger moment of inertia. As a result, the values of P_{CN} slightly differ from those calculated with $J = 0$. In order to calculate $\sigma_c(E_{\rm c.m.}, J)$ in (1) the simple expression $\sigma_c(E_{\rm c.m.}, J) = \pi\lambda\!\!\!^{-2}(2J+1)T(E_{\rm c.m.}, J)$ is often used ($\lambda\!\!\!^{-}$ is the reduced de Broglie wavelength). The transmission coefficient $T(E_{\rm c.m.}, J)$ through the Coulomb barrier restricts also the angular momentum range. The weight function $(2J+1)P_{CN}(E_{\rm c.m.}, J)$ used to obtain σ_{CN} has its maximum at $J = 20\hbar$. Since the calculation of σ_{CN} is of interest to determine the evaporation residues cross sections, only low angular momenta can be considered. Indeed, the surviving probabilities of the compound nuclei in the reactions considered are narrow functions peaking at all energies at J values in the vicinity of zero [8]. Although the precise calculation of the excitation function demands the dependence of P_{CN} on J, for the estimations of the evaporation residues cross sections, we can use the values of σ_{CN} calculated with $J_{max} = 10 - 15\hbar$ and $P_{CN}(E_{\rm c.m.}, J = 0)$ with a good accuracy.

III. RESULTS AND DISCUSSIONS

A. Effect of transient times

Since the difference between B^*_{fus} and B_{qf} and their absolute values can be large in some reactions, the role of the transient time in the calculation of P_{CN} and t_0 should be estimated. The motions in R and η are close to the underdamped and overdamped motions, respectively. Therefore, the transient time for the realistic values of Γ can be estimated by the expressions [13]

$$\tau_R = \frac{\hbar}{\Gamma} \ln(10B_{qf}/T), \tag{10}$$

$$\tau_\eta = \frac{\Gamma}{2\hbar\omega_\eta^2} \ln(10B^*_{fus}/T), \tag{11}$$

The calculated time dependences $\lambda_\eta(t)$ with Eq. (24) in [12] are presented in Fig. 4 for the reactions ^{90}Zr+^{90}Zr and ^{136}Xe+^{136}Xe at $\Gamma = 2$ MeV and $E^* = 30$ MeV. We find that the transient times taken from Fig. 4 are practically the same as the ones calculated with (11). The calculated transient times and life-times for different systems are given in Table 1. One can see that the transient stage does practically not effect the values of t_0.

It is known [27] that the consideration of the transient stage is important for large excitation energies when the particle emission change the system during the fission or fusion time. However, this is not so in our cases and the calculation with the transient time (Table 2) leads only to a decrease of P_{CN} by maximal 30% in the reactions ^{136}Xe+^{136}Xe and ^{110}Pd+^{136}Xe in comparison with the value of P^0_{CN} in (5) for $\Gamma = 2$ MeV. In other reactions considered the effect of the transient stage is negligible. Therefore, we can neglect the transient time in the calculations of P_{CN} for the most considered reactions. For the reactions with $B^*_{fus} - B_{qf} \geq 15$ MeV, the values of P_{CN} are small and the corrections ΔP_{CN} from the transient stage are practically within the accuracy of the calculated barrier heights. In these reactions the values of P_{CN} calculated without ΔP_{CN} in (5) are the upper limits of the fusion probabilities and can also be used for estimations of fusion cross sections.

B. Large excitation energies of the DNS

The values of P_{CN} (Table 3) are in agreement for most of the reactions with the ones extracted from the experimental data [7,28,29] and with the results of our previous calculations [1,11]. For example, for the reactions ^{90}Zr+^{90}Zr, ^{100}Mo+^{100}Mo, and ^{110}Pd+^{110}Pd the values of $P_{CN} \approx 4 \times 10^{-1},\ 10^{-2},\ 10^{-4}$, respectively, yield a good agreement with the experimental data of $\sigma_{CN}(E_{\rm c.m.})$. For the ^{110}Pd+^{110}Pd reaction, the value of $\sigma_{CN}(E_{\rm c.m.})$ calculated with the macroscopic dynamical model [1] is about three orders of magnitude larger than the experimental one. Thus, the competition between the complete fusion and quasifission processes is extremely important in the DNS evolution. Perhaps, due to the small value of P_{CN} in the ^{110}Pd+^{136}Xe reaction, the fusion was not observed in [29].

The values of P_{CN} can be also calculated from (2) by using the one–dimensional Kramers-type expression instead of Eq. (8):

$$\lambda_i^{Kr} = \frac{1}{2\pi}\frac{\omega_i}{\omega_i^{B_i}}\left(\sqrt{\left(\frac{\Gamma}{2\hbar}\right)^2 + \left(\omega_i^{B_i}\right)^2} - \frac{\Gamma}{2\hbar}\right)\exp\left[-\frac{B_i}{T}\right]. \qquad (12)$$

We approximately find the same results with this formula as with Eq. (8). Therefore, the estimations of the transient times with (10) and (11) are realistic.

In addition to the reactions presented in Table 3 the fusion probabilities were calculated for the reactions ^{96}Zr+^{124}Sn and ^{124}Sn+^{124}Sn with $\Gamma = 2$ MeV, $J = 0$ and the DNS excitation energy 30 MeV. The values of P_{CN} as a function of $Z_1 \times Z_2$ (Z_1 and Z_2 are the charge numbers of the colliding nuclei) are presented in Fig. 5. One can see the exponential decrease of the fusion probability with increasing $Z_1 \times Z_2$ in the symmetric and almost symmetric reactions. Therefore, the experimentally observed [8] rapid fall-off of the fusion cross sections with increasing $Z_1 \times Z_2$ is simply explained in our model.

The fusion and quasifission rates decrease with increasing Γ. However, P_{CN} increases quickly (the quasifission rate decreases more strongly than the fusion rate) and reaches a plateau at $\Gamma \approx 4$MeV because the changes of the dissipative effects in η and R variables start to compensate each other. The calculated dependence of λ_η^{Kr}, λ_R^{Kr} and P_{CN} on the friction

parameter Γ is shown in Fig. 6 for the ^{110}Pd+^{110}Pd reaction. Since the fusion probability increases not much with Γ, our calculations agree with the values of P_{CN} obtained within the approach [1] based on statistical assumptions within an order of magnitude. It is seen that the results of the calculations are not crucial to the exact value of the parameter Γ for $\Gamma > 2$ MeV. A realistic value of the parameter Γ is about 2 MeV. This value should be used in the further calculations.

The dependences of P_{CN} on the excitation energy $E^* = E_{\rm c.m.} - V(R_m)$ of the DNS are given for the ^{110}Pd+^{110}Pd and ^{86}Kr+^{136}Xe reactions in Fig. 7. We observe that P_{CN} increases with E^* because the value of λ_R^{Kr} in (2) increases slower than λ_η^{Kr} grows. For the ^{86}Kr+^{136}Xe reaction, the P_{CN} values were calculated for two cases. In the first case, liquid drop masses in (9) and spherical nuclei in the DNS were used to calculate B^*_{fus} and B_{qf}. In the second case, realistic masses in (9), spherical nuclei in the initial DNS and a deformed heavy nucleus in the ground state near $\eta = \eta_{BG}$ were taken. The pole orientation of the nuclei leads to the minimum of the potential energy in the DNS. Due to the deformation effect near $\eta = \eta_{BG}$, the value of $V(R_m)$ decreases as compared to the calculation with the spherical nuclei and $U(R_m, \eta_{BG})$ decreases. As a result, B^*_{fus} decreases and P_{CN} increases (Fig. 7). The driving potential with realistic binding energies and deformation effects is preferable for small excitation energies. The driving potential with the liquid drop binding energies is good for large excitation energies. For the $5n$ channel in the ^{86}Kr+^{136}Xe reaction, the excitation energy of the compound nucleus is about 46 MeV ($E^* = 30$ MeV) and $P_{CN} = 4\times10^{-2}$. With $\sigma_c = 23$ mb estimated with the model [3] and average value of $< \Gamma_n/\Gamma_f >= 0.3$ taken from Ref. [30], we obtain the evaporation residue cross section $\sigma_{ER} \approx \sigma_c P_{CN} < \Gamma_n/\Gamma_f >^5 = 2.2$ μb which is in agreement with the experimental value 5 μb [31].

The energy threshold for complete fusion is related to the fusion barrier B^*_{fus} (see Table 3) and can be much smaller than the extra-extra push energy which, for example, is $E_{\rm xx}$= 60 MeV and 30 MeV in ^{110}Pd+^{110}Pd and ^{62}Ni+^{208}Pb reactions, respectively, predicted in the macroscopic dynamical model [2]. This result of our model is in agreement with recent experimental data on the synthesis of the new superheavy elements [5,6].

C. Small excitation energies of the DNS

For low excitation energies of the initial DNS in asymmetrical reactions ^{62}Ni+^{208}Pb $\rightarrow^{270}$ 110, ^{70}Zn+^{208}Pb $\rightarrow^{278}$ 112, ^{82}Se+^{208}Pb $\rightarrow^{290}$ 116, and ^{48}Ca+^{244}Pu $\rightarrow^{292}$ 114 which were used for the synthesis of new superheavy elements, the initial DNS is in the local minimum of $U(\eta)$ due to shell effects (realistic binding energies are taken in (9)) [11]. In this case, we can use the Kramers–type expressions (8) to estimate the values of P_{CN} (Table 4). For these reactions, deformations of the DNS nuclei were taken into account [11,12]. Since in the ^{48}Ca+^{244}Pu reaction the heavy nucleus is deformed even in the initial DNS, the treatment of the deformation of nuclei leads to larger values of B^*_{fus} as compared to the calculation with spherical nuclei (Table 4). Deformation effects lead to a decrease of B^*_{fus} in other reactions. The detailed discussion of the influence of the deformation and orientation of the DNS nuclei on the value of B^*_{fus} is given in [12]. In the reactions leading to the superheavy nuclei only partial waves with very small J up to $J_{max} = 10 - 15\hbar$ contribute the evaporation residue cross section because these nuclei are instable against fission for larger J. The effect of the transient time in these reactions seems to be very small.

Using the results presented in Table 4 one may explain the smaller fusion yields of the nuclei with $Z = 112$ as compared to the fusion yields of the nuclei with $Z = 110$ [6]. As given in Table 4, the probability to obtain a superheavy nucleus with $Z = 116$ in the ^{82}Se+^{208}Pb reaction is very small. The use of this combination for producing heavy compound nuclei with a small excitation energy may be problematic. In spite of the larger value of P_{CN} in the ^{48}Ca+^{244}Pu reaction as compared with others in Table 4, the compound nucleus seems to be more excited due to the Q–value. The analysis of the surviving probability W_{sur} of the compound nucleus is extremely important to estimate the yield of the element with $Z = 114$ in this reaction.

By comparing P_{CN} in Tables 3 and 4 with P_{CN} given in the experimental work, we should bear in mind that the experimental values were extracted from the evaporation residues cross sections $\sigma_{ER}(E_{\rm c.m.})$ by model assumptions about the surviving probability

W_{sur} of the excited compound nucleus ($\sigma_{ER} = \sigma_c\, P_{CN}\, W_{sur}$) [1,28]. For the 1n channel in the ^{62}Ni+^{208}Pb reaction, the excitation energy of the compound nucleus is about 13 MeV and $P_{CN} = 7 \times 10^{-6}$. Extrapolating the systematic representation in Refs. [30,32] for the nucleus ^{270}110 we estimated $W_{sur} \approx \Gamma_n/\Gamma_f = 3 \times 10^{-4}$. With $\sigma_c = 4$ mb estimated with the optical model [3] and the values of P_{CN} and W_{sur}, we obtain $\sigma_{ER} = 8.4$ pb which is in agreement with the experiment [5].

A discussion on the accuracy of the model presented is necessary for applying it to reactions producing superheavy elements with very small cross sections. As in any model, certain assumptions are used in our approach. However, with the same assumptions and the set of the parameters our model is able to describe the experimental data for different reactions. As it is seen, our model gives good results for the ^{90}Zr+^{90}Zr reaction for which the known traditional models are applicable. However, our model describes also the experimental data well in the case of reactions where the fusion cross sections are very small and other models may fail [1].

IV. SUMMARY

The new model suggested to calculate the probability of the fusion of heavy nuclei is useful for the analysis of experimental data. The results obtained support the use of the simple statistical assumptions of our previous studies [1,11]. A good description of P_{CN} in our model can be considered as an evidence for the DNS–concept providing a realistic interpretation of the mechanism of fusion process. In our opinion the fusion probability is small in many reactions with heavy nuclei because quasifission plays a major role. Without taking the quasifission into account, the explanation of the experiments on the fusion of heavy nuclei is not possible. Based on the results presented, we plan calculations of the evaporation residues cross sections for a large set of reactions used to produce the superheavy elements.

ACKNOWLEDGMENTS

We thank Dr. E.Cherepanov, Dr. A.Nasirov (Dubna) and Dr. S.Hofmann (Darmstadt) for fruitful discussions. The authors (G.G.A. and N.V.A.) are grateful to the Justus–Liebig–Universität Giessen for the hospitality and financial support. This work was supported in part by the Russian Foundation for Basic Research under Grants N 95–02–05684, N 95–02–05975, and DFG. One of the authors (N.V.A.) thank the Alexander von Humboldt Foundation for the support during the completion this work.

REFERENCES

[1] N.V.Antonenko, E.A.Cherepanov, A.V.Nasirov, V.B.Permjakov and V.V.Volkov, Phys. Lett. B 319 (1993) 425; Phys. Rev. C 51 (1995) 2635; E.A.Cherepanov, V.V.Volkov, N.V.Antonenko, V.B.Permjakov and A.V.Nasirov, Nucl. Phys. A 583 (1995) 165.

[2] W.J. Swiatecki, Prog. Particle and Nucl. Phys. 4 (1980) 383; Phys. Scripta 24 (1981) 113; S.Bjornholm and W.J.Swiatecki, Nucl. Phys. A 391 (1982) 471; J.P.Blocki, H.Feldmeier and W.J.Swiatecki, Nucl. Phys. A 459 (1986) 145.

[3] A.S. Iljinov, Yu.Ts. Oganessian and E.A. Cherepanov, Sov. J. Nucl. Phys. 36 (1982) 118.

[4] D.H.E. Gross, R.C. Nayak and L. Satpathy, Z. Phys. A 299 (1981) 63; P. Fröbrich, Phys. Rep. 116 (1984) 337; J. Marten and P. Fröbrich, Nucl. Phys A 545 (1992) 854.

[5] S. Hofmann, V. Ninov, F.P. Hessberger, P. Armbruster, H. Folger, G. Münzenberg, H.J. Schott, A.G. Popeko, A.V. Eremin, A.N. Andreev, S. Saro, R. Janic and M. Leino, Z. Phys. A 350 (1995) 277; Z. Phys. A 350 (1995) 281.

[6] S. Hofmann et al., Z. Phys. A 354 (1996) 229.

[7] W.Morawek, T.Ackermann, T.Brohn, H.G.Clerc, U.Gollerthan, E.Hanlet, M.Horz, W.Schwab, B.Voss, K.H.Schmidt, J.J.Gaimard, F.P.Hessberger, in: GSI Scientific Report (GSI, 1988) p.38; K.H.Schmidt, W.Morawek, Rep. Prog. Phys. 54 (1991) 949; W.Morawek, T.Ackermann, T.Brohn, H.G.Clerc, U.Gollerthan, E.Hanlet, M.Horz, W.Schwab, B.Voss, K.H.Schmidt and F.P.Hessberger, Z. Phys. A 341 (1991) 75.

[8] P.Armbruster, Ann. Rev. Nucl. Part. Sci. 35 (1985) 135.

[9] V.V.Volkov, Proc. Intern. School-Seminar on Heavy Ion Physics (Dubna, 1986), D7-87-68 (JINR, Dubna, 1987) p.528; Izv. AN SSSR ser. fiz. 50 (1986) 1879; in: Proc. of the 6th Intern. Conf. on Nuclear Reaction Mechanisms (Varenna, Italy 1991), ed. E.Gadioli (Ricerca Scientifica ed Educazione Permanente Supplemento n. 84, 1991) p.39.

[10] V.V. Volkov, Nuclear reactions of deep inelastic transfers (Energoizdat, Moscow, 1982); W.U. Schröder and J.R. Huizenga, *in* Treatise on Heavy-Ion Science, ed. D.A. Bromley, v.2 (New York, Plenum Press, 1984) p. 115.

[11] V.V.Volkov, E.A.Cherepanov, N.V.Antonenko and A.V.Nasirov, in: Proc. Int. Conf. on Low Energy Nuclear Dynamics, St.Petersburg, 1995, eds. Yu.Oganessian, R.Kalpakchieva, W. von Oertzen (World Scientific, Singapore, 1995) p. 336.

[12] G.G.Adamian, N.V.Antonenko and W.Scheid, Nucl. Phys. A 618 (1997) 176.

[13] K.H. Bhatt, P. Grange and B. Hiller, Phys. Rev. C 33 (1986) 954; P. Grange, Nucl. Phys. A 428 (1984) 37c.

[14] H.A. Kramers, Physica. 7 (1940) 284.

[15] V.M. Strutinsky, Phys. Lett. B 47 (1973) 121; H. Hofmann and J.R. Nix, Phys. Lett. B 122 (1983) 117; P. Grange, Jun-Qing Li and H.A. Weidenmüller, Phys. Rev. C 27 (1983) 2063; P. Fröbrich and G.R. Tillack, Nucl. Phys. A 540 (1992) 353.

[16] H.A. Weidenmüller, Jing-Shang Zhang, J. Stat. Phys. 34 (1984) 191.

[17] G.G.Adamian, N.V.Antonenko, R.V.Jolos and A.K.Nasirov, Phys. Part. & Nucl. 25 (1994) 583; Nucl. Phys. A 551 (1993) 321; N.V.Antonenko, S.P.Ivanova, R.V.Jolos and W.Scheid, Phys. Rev. C 50 (1994) 2063.

[18] H.J.Fink, J.Maruhn, W.Scheid and W.Greiner, Z. Phys. A 268 (1974) 321; J.Maruhn, W.Scheid and W.Greiner, in: Heavy ion collisions, ed. R. Bock, v. 2 (North-Holland, Amsterdam, 1980).

[19] G.G.Adamian, N.V.Antonenko, R.V.Jolos and W.Scheid, Nucl. Phys. A (1997) in print.

[20] I.I.Gonchar and G.I.Kosenko, Sov. J. Nucl. Phys. 53 (1991) 133.

[21] H.Hofmann and P.J.Siemens, Nucl. Phys. A 257 (1976) 165; R.Samhammer, H.Hofmann and S.Yamaji, Nucl. Phys. A 503 (1989) 404.

[22] G.G.Adamian, N.V.Antonenko and R.V.Jolos, Nucl. Phys. A 584 (1995) 205.

[23] A.M. Wapstra and G. Audi, Nucl. Phys. A 440 (1985) 327.

[24] G.G.Adamian, N.V.Antonenko, R.V.Jolos, S.P.Ivanova and O.I.Melnikova, Int. J. Mod. Phys. E 5 (1996) 191.

[25] S.Raman, C.H.Malarkey, W.T.Milner, C.W.Nestor and P.H.Stelson, At. Data Nucl. Data Tables 36 (1987) 1.

[26] N.V.Antonenko, G.G.Adamain, V.V.Volkov, E.A.Cherepanov and A.V.Nasirov, in: Proc. Int. Conf. Nuclear Structure at the Limits, Argonne, 1996, (ANL, 1997) in print.

[27] K.Pomorski, J.Bartel, J.Richert and K.Dietrich Nucl. Phys. A 605 (1996) 87.

[28] P.Armbruster, in: Proc. Intern. School-Seminar on Heavy Ion Physics (Dubna, 1986), D7-87-68 (JINR, Dubna, 1987) p. 82.

[29] H. Gaggeler, T. Sikkeland, G. Wirth, W. Bruchle, W. Brugl, G. Franz, G. Herrmann, J.V. Kratz, M. Schaedel, K. Summerer and W. Weber, Z. Phys. A 316 (1984) 291; Nucl. Phys. A 275 (1977) 464.

[30] G.Münzenberg, Rep. Prog. Phys. 51 (1988) 57.

[31] C. Stodel, S. Hofmann, F.P.Hessberger, V.Ninov, R.N.Sagaidak, A.G.Popeko, Yu.Ts.Oganessian, A.Yu.Lavrentjev, A.V.Eremin, in: GSI Scientific Report (GSI, 1996) p.17.

[32] R.Vandenbosch and J.R.Huizenga, Nuclear Fission (New York, Academic, 1973).

TABLES

TABLE I. Calculated transient times (10) and (11), quasistationary values of $1/\lambda_i^{Kr}$ and life time (6) in the symmetric and almost symmetric reactions for $J = 0$, $\Gamma = 2$ MeV and the excitation energy $E^* = 30$ MeV of the initial DNS. The calculations were made with B^*_{fus} and B_{qf} given in Table 3.

Reactions	τ_R $\times 10^{-21}$s	$1/\lambda_R^{Kr}$ $\times 10^{-21}$s	τ_η $\times 10^{-21}$s	$1/\lambda_\eta^{Kr}$ $\times 10^{-19}$s	t_{00} $\times 10^{-21}$s	Δt $\times 10^{-21}$s
^{90}Zr+^{90}Zr	1.2	104	2.4	1.6	63	1.0
^{100}Mo+^{100}Mo	1.1	60	2.8	39	58	0.6
^{110}Pd+^{110}Pd	1.0	32	3.1	2800	32	0.6
^{86}Kr+^{136}Xe	1.1	70	2.8	18	68	0.6
^{110}Pd+^{136}Xe	0.5	50	3.2	8300	5	0.3
^{136}Xe+^{136}Xe	0.5	50	3.5	7.1×10^6	5	0.3

TABLE II. Calculated values of P^0_{CN}, ΔP_{CN} and the ratio $\Delta P_{CN}/P^0_{CN}$ (see Eq. (6)) in the symmetric and almost symmetric reactions for $J = 0$, $\Gamma = 2$ MeV and the excitation energy $E^* = 30$ MeV of the initial DNS. The calculations were made with B^*_{fus} and B_{qf} given in Table 3.

Reactions	P^0_{CN}	ΔP_{CN}	$\Delta P_{CN}/P^0_{CN}$
^{90}Zr+^{90}Zr	4.0×10^{-1}	2.7×10^{-3}	6.7×10^{-3}
^{100}Mo+^{100}Mo	1.5×10^{-2}	2.6×10^{-4}	1.7×10^{-2}
^{110}Pd+^{110}Pd	1.1×10^{-4}	4.2×10^{-6}	3.8×10^{-2}
^{86}Kr+^{136}Xe	4.0×10^{-2}	5.6×10^{-4}	1.4×10^{-2}
^{110}Pd+^{136}Xe	5.5×10^{-6}	1.7×10^{-6}	3.1×10^{-1}
^{136}Xe+^{136}Xe	6.1×10^{-9}	1.9×10^{-9}	3.1×10^{-1}

TABLE III. Calculated fusion probability P_{CN} in the symmetric and almost symmetric reactions for different friction parameters Γ. The calculations were made for $J = 0$ and the excitation energy $E^* = 30$ MeV of the initial DNS. For the calculated values of P_{CN}, liquid drop masses and spherical nuclei in the DNS were used in (9).

Reactions	B^*_{fus} (MeV)	B_{qf} (MeV)	P_{CN}				
			Γ=0 MeV	Γ=1 MeV	Γ=2 MeV	Γ=3 MeV	Γ=4 MeV
^{90}Zr+^{90}Zr	6	5	3.1×10^{-1}	3.6×10^{-1}	4.0×10^{-1}	4.5×10^{-1}	4.8×10^{-1}
^{100}Mo+^{100}Mo	10	4	8.3×10^{-3}	1.0×10^{-2}	1.5×10^{-2}	1.8×10^{-2}	2.0×10^{-2}
^{110}Pd+^{110}Pd	15	3	6.5×10^{-5}	7.9×10^{-5}	1.1×10^{-4}	1.4×10^{-4}	1.5×10^{-4}
^{86}Kr+^{136}Xe	8.5	4	2.3×10^{-2}	2.7×10^{-2}	4.0×10^{-2}	5.0×10^{-2}	5.6×10^{-2}
^{110}Pd+^{136}Xe	15.5	0.5	9.0×10^{-7}	2.2×10^{-6}	3.8×10^{-6}	4.4×10^{-6}	5.0×10^{-6}
^{136}Xe+^{136}Xe	22.5	0.5	1.6×10^{-9}	2.5×10^{-9}	4.2×10^{-9}	4.9×10^{-9}	5.7×10^{-9}

TABLE IV. The same as in Table 3, but for asymmetric reactions used for producing superheavy nuclei. The deformation effects are taken into account (see text). The calculations were made for $J = 0$ and the excitation energy $E^* = 15$ MeV of the initial DNS with exception of the ^{48}Ca+^{244}Pu reaction. For the ^{48}Ca+^{244}Pu reaction, the choice of the initial excitation energies in the calculations of P_{CN} with ($E^* = 33$ MeV) and without ($E^* = 15$ MeV) deformation effects (sph.) yields the same excitation energy of the compound nucleus (≈ 40 MeV).

Reactions	B^*_{fus} (MeV)	B_{qf} (MeV)	P_{CN}				
			Γ=0 MeV	Γ=1 MeV	Γ=2 MeV	Γ=3 MeV	Γ=4 MeV
^{62}Ni+^{208}Pb $\rightarrow^{270}$ 110	8	1.5	1.4×10^{-4}	1.6×10^{-4}	2.2×10^{-4}	2.9×10^{-4}	3.2×10^{-4}
^{70}Zn+^{208}Pb $\rightarrow^{278}$ 112	9.5	1	9.1×10^{-6}	1.1×10^{-5}	1.5×10^{-5}	1.9×10^{-5}	2.2×10^{-5}
^{82}Se+^{208}Pb $\rightarrow^{290}$ 116	12.5	0.5	9.4×10^{-8}	1.1×10^{-7}	1.5×10^{-7}	1.9×10^{-7}	2.2×10^{-7}
^{48}Ca+^{244}Pu $\rightarrow^{292}$ 114	12	4	3.7×10^{-4}	4.4×10^{-4}	6.2×10^{-4}	8.0×10^{-4}	9.1×10^{-4}
(sph.) ^{48}Ca+^{244}Pu $\rightarrow^{292}$ 114	7	3	2.3×10^{-3}	2.8×10^{-3}	3.9×10^{-3}	5.0×10^{-3}	5.6×10^{-3}

FIGURES

FIG. 1. Calculated potential energy of the DNS corresponding to the ^{180}Hg compound nucleus as a function of the mass asymmetry for zero angular momentum (upper part). The energy scales are normalized to the total energy of the compound nucleus. Liquid drop binding energies are used in (9). Calculated nucleus-nucleus potential in the ^{90}Zr+^{90}Zr reaction for zero angular momentum (bottom part).

FIG. 2. Calculated potential energy of the DNS in the ^{86}Kr+^{136}Xe reactions as a function of η for $J = 0$. The result calculated with liquid drop binding energies in (9) is presented by the dashed line. The driving potentials with and without deformation effects in the DNS, obtained with realistic binding energies in (9), are presented by thick and thin lines, respectively. The deformed nuclei of the DNS are assumed in the pole orientation.

FIG. 3. Dependences of B_{qf}, B^*_{fus}, P_{CN} and $(2J+1)P_{CN}$ on J for the reactions ^{90}Zr+^{90}Zr (solid lines) and ^{110}Pd+^{110}Pd (dashed lines). In the calculations of P_{CN} the values $E^* = 30$ MeV and $\Gamma = 2$ MeV are used.

FIG. 4. Calculated fusion rates λ_η as a function of time for the reactions ^{90}Zr+^{90}Zr (solid line) and ^{136}Xe+^{136}Xe (dashed line) at $E^* = 30$ MeV and $\Gamma = 2$ MeV.

FIG. 5. Calculated values (solid points) of the fusion probability as a function of $Z_1 \times Z_2$ for the reactions presented in Table 3 and the reactions ^{96}Zr+^{124}Sn ($B^*_{fus} = 9$ MeV, $B_{qf} = 4$ MeV) and ^{124}Sn+^{124}Sn ($B^*_{fus} = 16$ MeV, $B_{qf} = 0.5$ MeV) at $J = 0$, $\Gamma = 2$ MeV and $E^* = 30$ MeV. Z_1 and Z_2 are the charge numbers of the colliding nuclei. The solid line is drawn to guide the eye.

FIG. 6. Fusion (long-dashed line) and quasifission (short-dashed line) rates $\lambda_i^{Kr}(i = \eta, R)$ and fusion probability P_{CN} (solid line) as a function of the friction parameter Γ for the ^{110}Pd+^{110}Pd reaction at $J = 0$.

FIG. 7. Fusion probability P_{CN} as a function of the excitation energy $E^* = E_{\rm c.m.} - V(R_m)$ of the initial DNS for the reactions ^{110}Pd+^{110}Pd (upper part) and ^{86}Kr+^{136}Xe (bottom part) at $J = 0$. The results were obtained by using liquid-drop masses and spherical nuclei (solid lines) and realistic masses and a deformed heavy nucleus (dashed line) in the DNS. The calculations were made with a friction parameter $\Gamma = 2$ MeV.

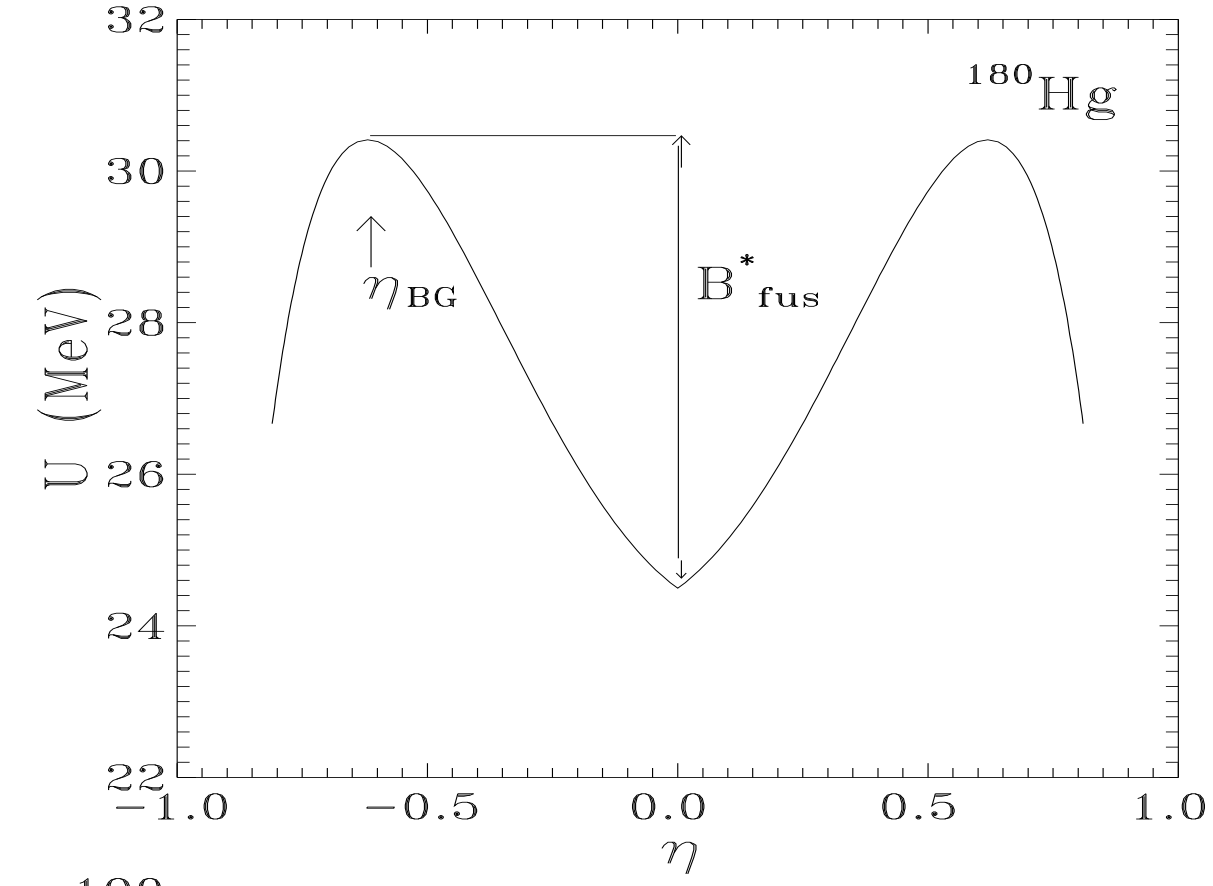
^{180}Hg
η_{BG}
B^*_{fus}
U (MeV)
η

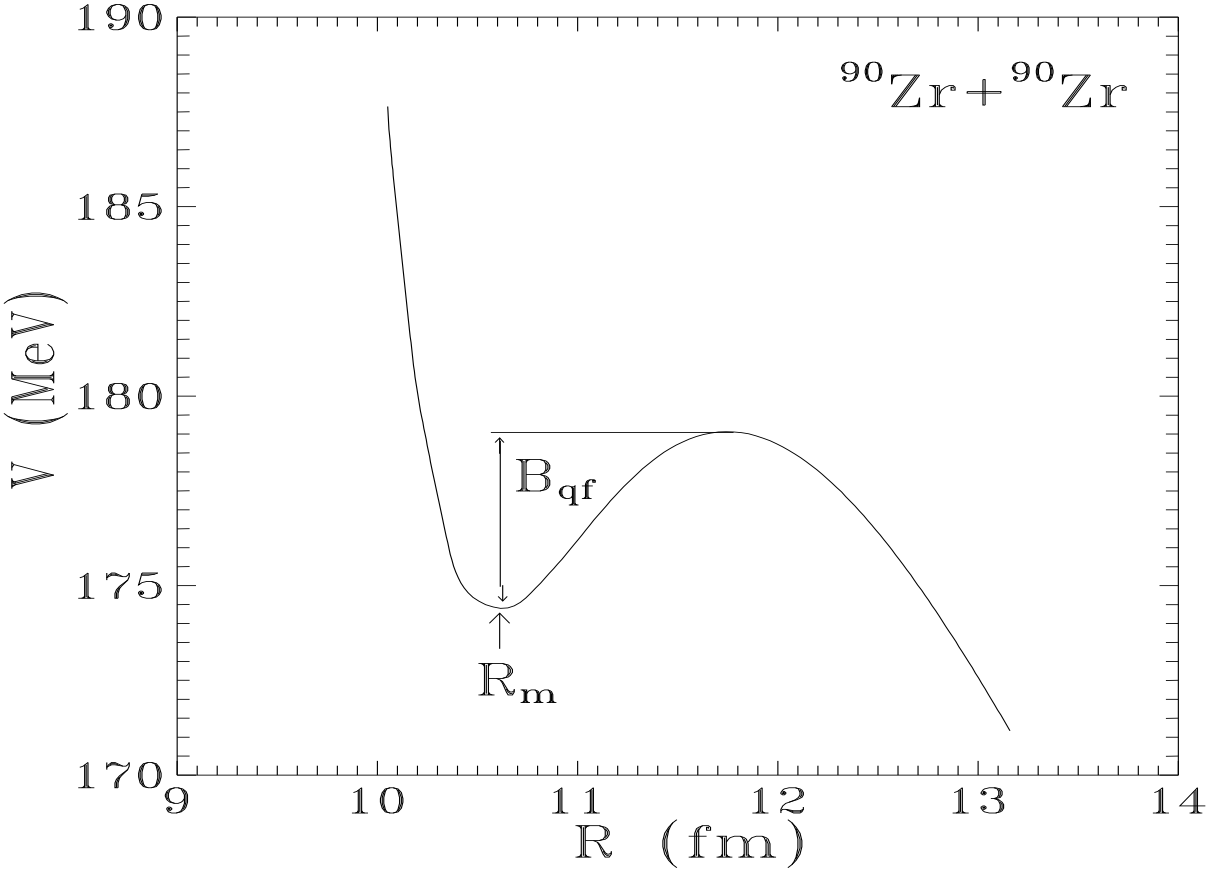
^{90}Zr+^{90}Zr
B_{qf}
R_m
V (MeV)
R (fm)

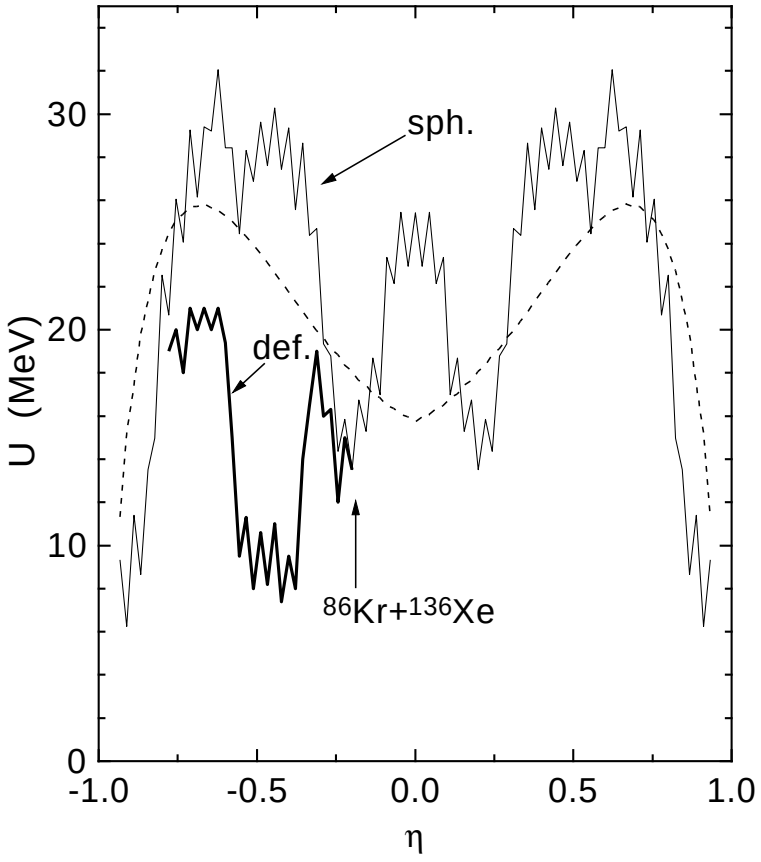

Fig.2 NUCPHA 1629

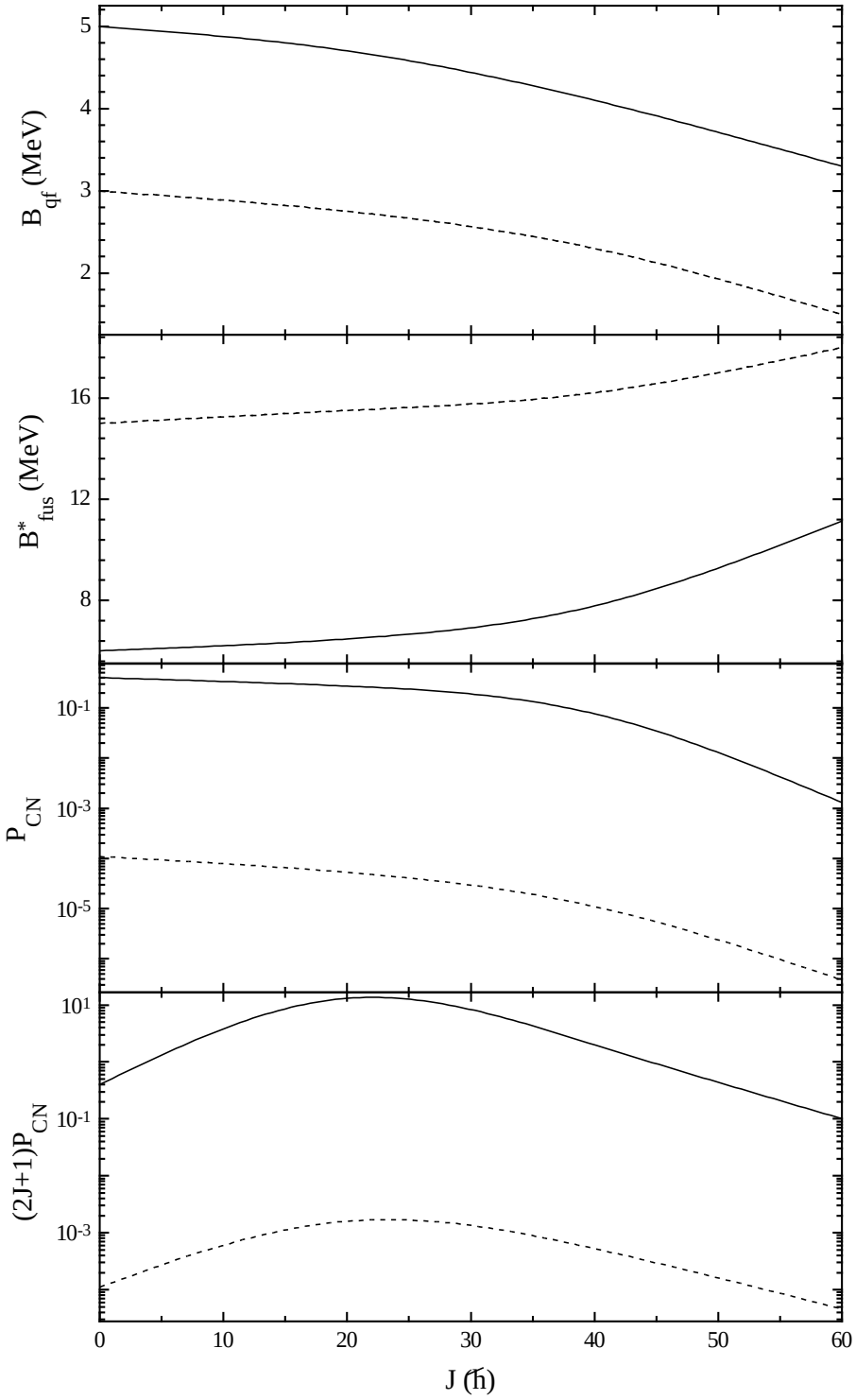

Fig.3 NUCPHA 1629

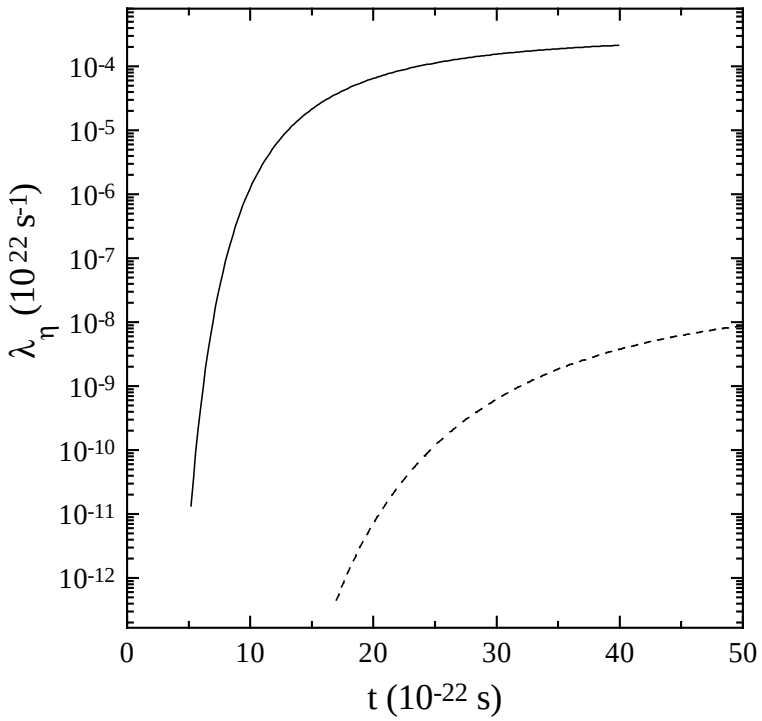

Fig.4 NUCPHA 1629

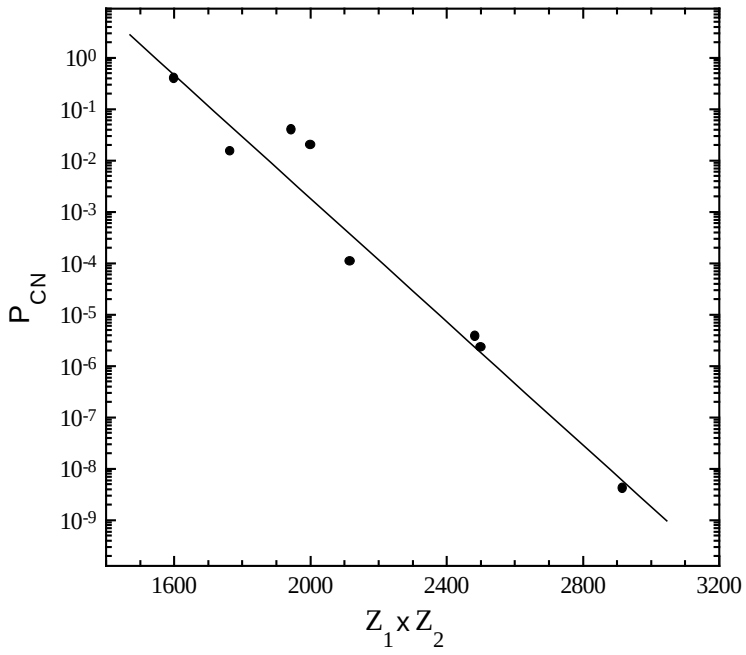

Fig.5. NUCPHA 1629

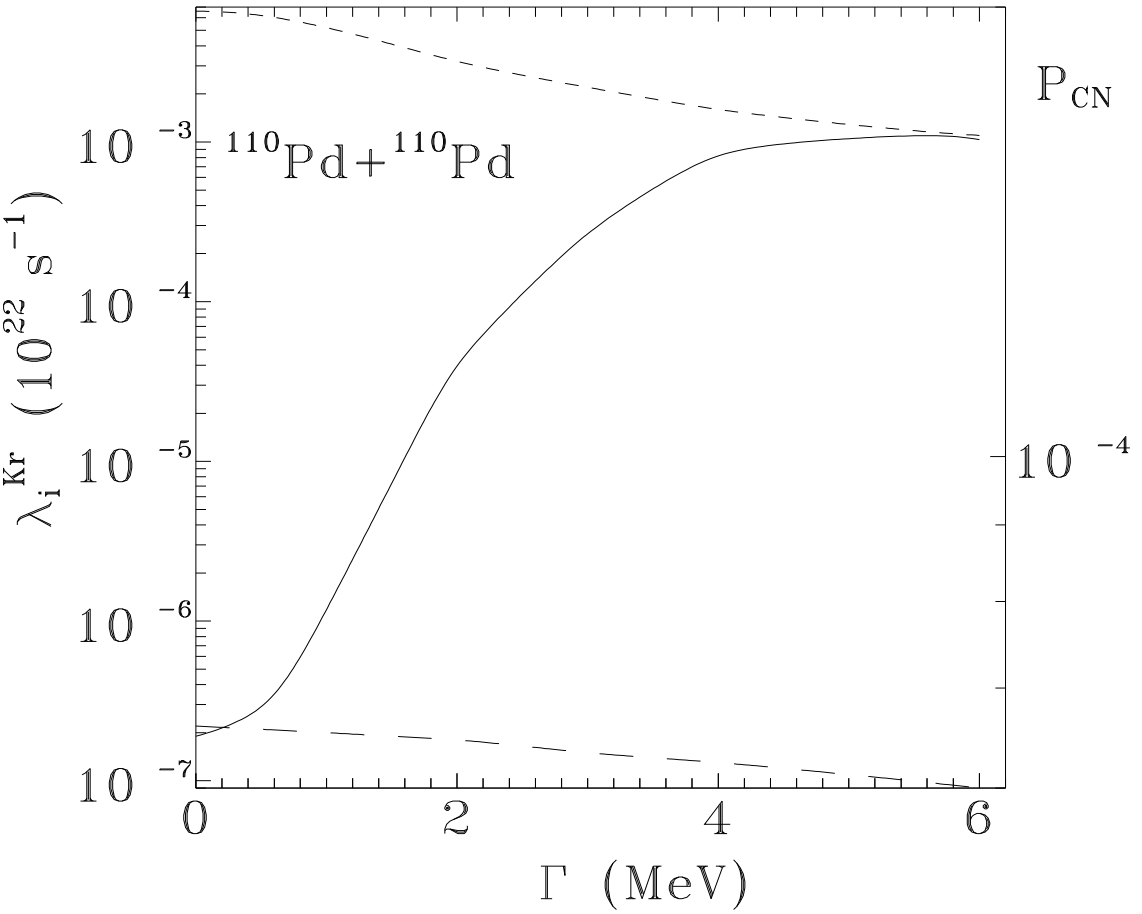
^{110}Pd+^{110}Pd
λ_i^{Kr} (10^{22} s^{-1})
P_{CN}
10^{-3}
10^{-4}
10^{-5}
10^{-6}
10^{-7}
10^{-4}
0
2
4
6
Γ (MeV)

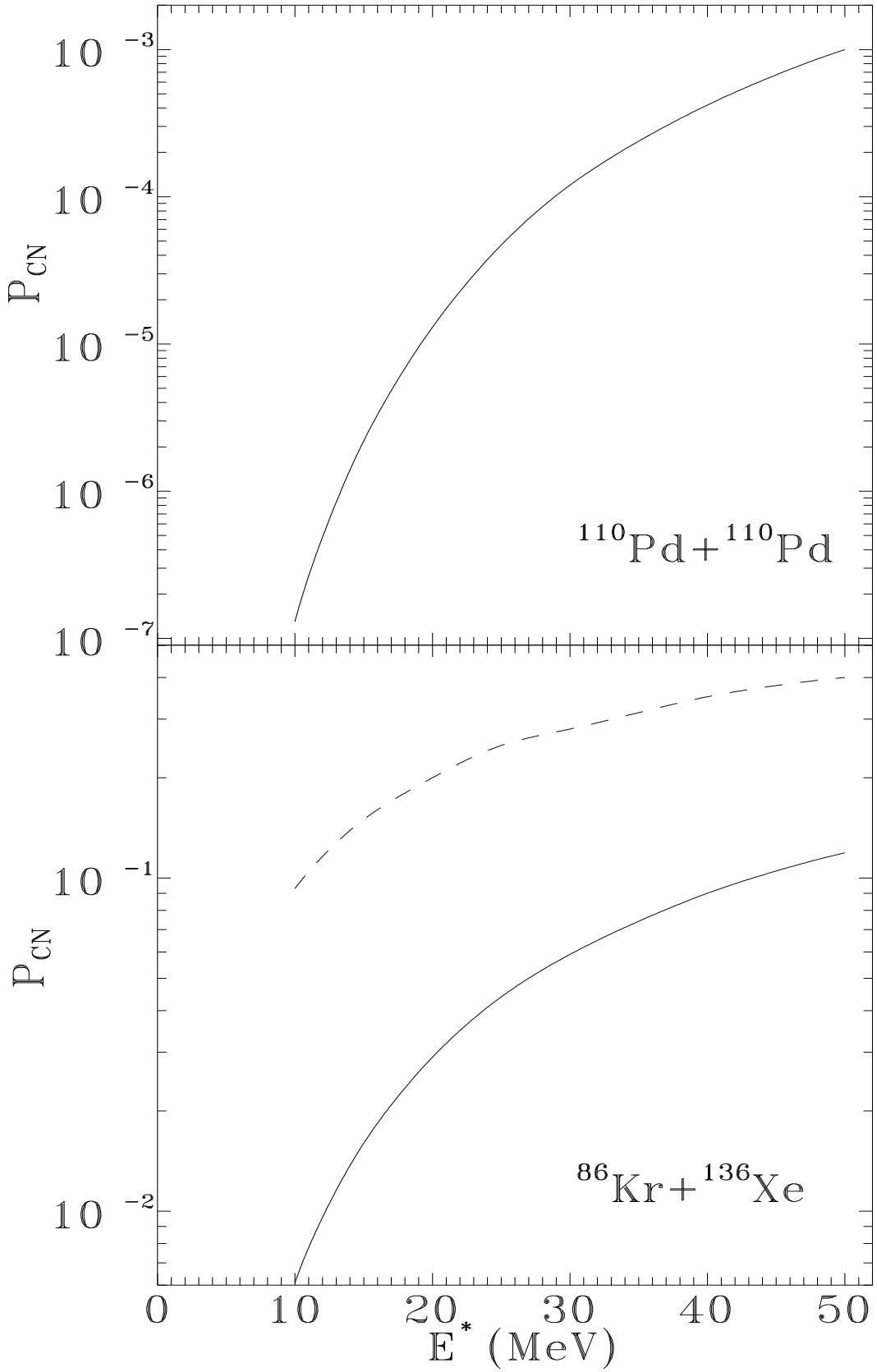
10^{-3}
10^{-4}
10^{-5}
10^{-6}
10^{-7}
P_{CN}
$^{110}Pd+^{110}Pd$
10^{-1}
10^{-2}
P_{CN}
$^{86}Kr+^{136}Xe$
0
10
20
30
40
50
E^* (MeV)